Turbulent heat transfer in a channel with bars in tandem and in side by side arrangements

Jaime Alvarez, Mirko Pap and Alvaro Valencia
Department of Mechanical Engineering, Univeridad de Chile, Santiago, Chile

Received May 2000
Revised September 2000
Accepted September 2000

Keywords *Numerical simulation, Turbulence, Heat transfer, Channels*

Abstract *This work numerically investigates the effects of two square bars placed in various arrangements in a channel on pressure drop and heat transfer. Tandem arrangements and the two bars arranged side by side to the approaching flow are considered. The separation distance between the bars is varied in both types of arrangements. The Reynolds number Re based on channel height is 10^4, whereas the bar height to channel height (d/H) is 0.152. The channel walls are subjected to a constant wall temperature. The k-ε turbulence model was used in conjunction with the Reynolds-averaged momentum and energy equations for the simulations. A finite volume technique with staggered grids combined with the SIMPLEC algorithm is applied with a fine grid resolution. Results show that the local and global Nusselt numbers on the channel walls are strongly increased by the unsteady vortex shedding induced by the bars.*

Nomenclature

A = Van Driest's constant (=26)
C_D = drag coefficient
C_f = skin friction coefficient on channel wall
C_L = lift coefficient
C_p = specific heat at constant pressure
C_μ, C_1, C_2 = k-ε turbulence model constants
d = bar height
D = drag
E = constant in wall function (=9)
f = apparent friction coefficient or frequency
f_o = apparent friction coefficient for the channel without bar
G_L = longitudinal spacing between bars' centers
G_T = transverse spacing between bars' centers
H = channel height
h(x) = local heat transfer coefficient
k = turbulent kinetic energy
L = channel length or lift
Nu = local Nusselt number, h(x) H / k
Nu_o = mean Nusselt number for the channel without bar
p = pressure
P_K = production of turbulent kinetic energy
Pr = Prandtl number υ/α (= 0.71)
Pr_t = turbulent Prandtl number (= 0.9)
q_w = wall heat flux
Re = Reynolds number, U_0H/υ
St = Strouhal number
t/T = phase of the periodic motion
T_B = bulk temperature
T_0 = inlet fluid temperature
T_W = channel wall temperature
T^+ = dimensionless temperature
Tu = turbulence level (=ú/U0)
U_0 = average velocity at the inlet
U^+ = dimensionless velocity
U = phase-averaged streamwise velocity
V = phase-averaged transverse velocity
y^+ = wall coordinate

The financial support received of Conicyt Chile under grant No. 1980695 is gratefully acknowledged.

Greek symbols

α = thermal diffusivity
β = velocity factor
$\triangle$ = difference
Γ = thermal diffusivity
Γ_t = turbulent thermal diffusivity
δ_{ij} = Kronecker delta
ε = dissipation rate of turbulent kinetic energy
κ = von Karman constant, (= 0.4)
μ = molecular viscosity
μ_t = turbulent viscosity
υ = kinematic viscosity
ρ = density
$\sigma_k, \sigma_\varepsilon$ = $k - \varepsilon$ turbulence model constants
τ = dimensionless time (=tU_0/H)
τ_w = wall shear stress

Introduction

The capacity to remove the heat generated by electronic components is one of the biggest restrictions for the design of these components. To address the issue of component cooling, the use of vortex generators is suggested to alter the flow on the channel walls and thereby increase the heat transfer. The design requires a thorough understanding of the influence of the interaction between unsteady vortex structures on heat transfer and flow loss. Most previous studies were related to a single circular cylinder or rectangular bar immersed in freestreams, while less studies were pertinent to flow passing through bars in confined ducts with different arrangements.

Durao *et al.* (1991) and Bosch *et al.* (1996) performed experimental studies of turbulent flow past a square bar placed at various distances from an adjacent wall. Durao *et al.* found the critical value for the gap beyond which vortex shedding occurs to be in the range G/D=0.25-0.5 bar heights at Re=13,600. For G/D=0.5 the main contribution to the normal stresses is the vortex shedding, so peaks of the normal stresses are located in the shear layers around the square bar. Bosch *et al.* at Re=22,000 observed steady flow for G/D=0.25, while vortex shedding was observed for G/D$\geq$0.5.

Bosch and Rodi (1999) reported calculations with two versions of the k-ε turbulence model for the flow passing a square bar at Re=22,000 placed at various distances from an adjacent wall. They obtained the unsteady shedding motion around the bar for G/D$\geq$0.5. The predictions of the unsteady velocity vectors for different phases agree good with the experimentally observed mean flow motion (Bosch *et al.*, 1996).

Nakagawa *et al.* (1999) conducted an experimental study of heat transfer in a turbulent channel flow with a rectangular bar having various width-to-height ratios, b/h, 0.5, 1, 2 and 3, and for three Reynolds numbers. Time-averaged heat transfer coefficients on the heated channel wall have been measured. They measured heat flux fluctuation with thin-film heat flux sensors in three points of the channel wall, and they used the smoke wire method for flow visualization. They conclude that the wall heat flux fluctuates in phase with the shedding vortices from the bar. The position of the maximum wall heat flux moves downstream as the shedding vortices travel through the channel, which results in extensive heat transfer enhancement.

Valencia (2000) performed a numerical study to compute the heat transfer and friction in a channel with a mounted square bar of different sizes detached

from the channel wall. The Reynolds number Re based on channel height ranges from 10^4 to 10^5, whereas the bar height to channel height (d/H) varies from 0.15 to 0.35. The channel walls are subjected to a constant wall temperature. The standard k-ε turbulence model and a modified version proposed by Launder and Kato (1993) were used in conjunction with the Reynolds-averaged momentum and energy equations for the simulations, and compared thereafter. The experimental results of Nakagawa *et al.* (2000) of the local Nusselt numbers were used for an evaluation of the performance of the used numerical methods and the k-ε turbulence model. The comparison of time averaged local Nusselt numbers distribution on the heated channel wall shows that the simulated heat transfer coefficients agree well with the experimental results except in the recirculation zone behind the bar. The differences can be explained by the inadequate experimental position of the bar for the simulation. Valencia compared the computed local heat transfer coefficient between the standard k-ε turbulence model and the modified version of the standard k-ε turbulence model proposed by Launder and Kato (1993), the differences among the Nusselt numbers calculated with LK model and standard k-ε model were small. Valencia also showed that the displacement of the bar from the channel axis toward the wall did not cause an increase in the global heat transfer coefficient on the channel walls compared with one bar centered in the channel.

Studies involving more than one detached bar arranged in a channel are seldom found in the available literature. For two bars in tandem, Tatsutani *et al.* (1993) performed dye visualization and numerical simulation to investigate the effect of the bar separation distance on the flow behavior and heat transfer of the downstream bar. The investigated Reynolds number based on bar height ranged between 200 and 1,600, the blockage ratio was 0.2, and the bar separation distance-height ratio was between 0.25 and 4. They found that at a critical inter-bar spacing related to Reynolds number the shedding of large eddies also occurs at the upstream bar and this results in a highly mixed inter-bar flow.

Cho *et al.* (1994) reported mass transfer measurements and smoke-wire flow visualization from an array of rectangular bars arranged side by side to the approaching flow. The local mass transfer coefficients indicate that the flow pattern is asymmetric in spite of using an array of two-dimensional, equally spaced identical bars. The flow shows alternate short and long wakes around the bars, due to the instability of vortex shedding.

On the contrary, the fluid flow around circular cylinders has been extensively studied. Zdravkovich (1977) presents a review of flow interference between two circular cylinders in various arrangements for different separation distances and Reynolds numbers. The flow past two identical circular cylinders in tandem reveals the existence of two distinct patterns above and below a critical cylinder separation of three diameters, from center to center. At low separations a vortex street is observed only in the wake of the downstream cylinder and the flow in the gap between the cylinders is essentially stagnant.

In this range the pressure at the rear of the upstream cylinder increases with increasing cylinder spacing, thus reducing the drag on the upstream cylinder. The gap side of the downstream cylinder has a very low negative pressure (called the gap pressure), corresponding to the value of the upstream cylinder's base pressure. This produces a negative drag or a thrust force on the downstream cylinder. Beyond the three diameter separation, vortex shedding by the upstream cylinder is also observed. This causes the gap pressure to jump to a significantly higher value, exceeding the value of the base pressure. Thus, a discontinuous increase in the drag coefficient of the downstream cylinder is registered, also the eddy shedding from the upstream cylinder strongly affects and synchronizes eddy shedding from the downstream cylinder.

In side by side arrangement to the approaching flow of two circular cylinders an interference in drag coefficient was observed for a separation distance smaller than five cylinder diameters. The flow patterns in side by side arrangements show a bistable nature. For a separation distance greater than two, the process of the vortex formation of both cylinders is exactly the same as that of the single cylinder. When the separation distance becomes smaller, the bulk flow between the two cylinders deflects, the deflection to one side or the other can equally take place. Owing to this phenomenon, the size of the vortex formation region and the vortex shedding frequency of two cylinders are different from each other (Ishigai *et al.*, 1972).

Until the present work, there was only one computational and experimental study on turbulent fluid flow in a channel with an array of bluff bodies aligned along the channel axis (Liou and Chen, 1998). They performed spatially periodic turbulent heat transfer and fluid flow measurements with LDV. The Reynolds number based on the channel hydraulic diameter, the pitch to rib-height ratio, and the rib-height to channel-height ratio were 2×10^4, 10, and 0.13 respectively.

The main objective of the present study is therefore to investigate the effects of the interaction between two mounted bars in tandem arrangements and with the two bars arranged side by side to the approaching flow on the developing turbulent flow and heat transfer on a channel by numerical simulations with the k-ε turbulence model.

Governing equations

The flow field in the channel is assumed to be unsteady, two-dimensional, non-isothermal, incompressible and turbulent, and the fluid is assumed to be Newtonian with constant properties. Following the concept of Reynolds decomposition, an instantaneous quantity can be separated into a mean value that contains the periodic fluctuation and the stochastic turbulent fluctuation. Replacing in the momentum equations are obtained averaged equations that contain products of turbulent velocity fluctuations. These Reynolds stresses appearing in the momentum equations are simulated by the statistical k-ε turbulence model (Launder and Spalding, 1974). The continuity, averaged

momentum and energy equations, together with the equations for the turbulent kinetic energy k, and dissipation rate ε, are used to describe the incompressible unsteady separated flow and heat transfer in a channel with a two built-in bars in the computational domain.

Continuity:

$$\frac{\partial(\rho \mathrm{U_j})}{\partial \mathrm{x_j}} = 0 \tag{1}$$

Momentum:

$$\rho\frac{\partial \mathrm{U_i}}{\partial \mathrm{t}} + \frac{\partial(\rho \mathrm{U_i U_j})}{\partial \mathrm{x_j}} = -\frac{\partial \mathrm{p}}{\partial \mathrm{x_i}} + \frac{\partial}{\partial \mathrm{x_j}}[(\mu + \mu_\mathrm{t})(\frac{\partial \mathrm{U_i}}{\partial \mathrm{x_j}} + \frac{\partial \mathrm{U_j}}{\partial \mathrm{x_i}}) - \frac{2}{3}\rho \mathrm{k}\delta_{\mathrm{i,j}}\,] \tag{2}$$

Energy:

$$\rho\frac{\partial \mathrm{T}}{\partial \mathrm{t}} + \frac{\partial(\rho \mathrm{U_j T})}{\partial \mathrm{x_j}} = \frac{\partial}{\partial \mathrm{x_j}}[(\Gamma + \Gamma_\mathrm{t})\frac{\partial \mathrm{T}}{\partial \mathrm{x_j}}] \tag{3}$$

where the turbulent viscosity μ_t and the turbulent diffusion coefficient Γ_t are given by:

$$\mu_\mathrm{t} = \rho\ \mathrm{c}_\mu\ \frac{k^2}{\varepsilon} \qquad \Gamma_\mathrm{t}\ = \frac{\mu_\mathrm{t}}{\mathrm{Pr_t}} \tag{4}$$

The turbulent kinetic energy k and its dissipation rate ε are computed from the standard k-ε model of Launder and Spalding (1974):

$$\rho\frac{\partial \mathrm{k}}{\partial \mathrm{t}} + \frac{\partial(\rho \mathrm{U_j k})}{\partial \mathrm{x_j}}\ =\ \frac{\partial}{\partial \mathrm{x_j}}[(\mu + \frac{\mu_\mathrm{t}}{\sigma_\mathrm{k}})\frac{\partial \mathrm{k}}{\partial \mathrm{x_j}}]\ +\ \mathrm{P_K}\ -\ \rho\varepsilon \tag{5}$$

$$\rho\frac{\partial \varepsilon}{\partial \mathrm{t}} + \frac{\partial(\rho \mathrm{U_j}\varepsilon)}{\partial \mathrm{x_j}}\ =\ \frac{\partial}{\partial \mathrm{x_j}}[(\mu + \frac{\mu_\mathrm{t}}{\sigma_\varepsilon})\frac{\partial \varepsilon}{\partial \mathrm{x_j}}]\ + \mathrm{c}_1\frac{\varepsilon}{\mathrm{k}}\mathrm{P_K}\ -\ \mathrm{c}_2\rho\frac{\varepsilon^2}{\mathrm{k}} \tag{6}$$

The standard version of the k-ε model calculates the production term $\mathrm{P_K}$ of k from:

$$\mathrm{P_K} = \frac{\mu_\mathrm{t}}{2}(\frac{\partial \mathrm{U_i}}{\partial \mathrm{x_j}} + \frac{\partial \mathrm{U_j}}{\partial \mathrm{x_i}})^2 \tag{7}$$

Launder and Kato (1993) proposed to replace the production expression in equation (5) by:

$$\mathrm{P_K} = \mu_\mathrm{t}\sqrt{\frac{1}{2}(\frac{\partial \mathrm{U_i}}{\partial \mathrm{x_j}} + \frac{\partial \mathrm{U_j}}{\partial \mathrm{x_i}})^2}\ \sqrt{\frac{1}{2}(\frac{\partial \mathrm{U_i}}{\partial \mathrm{x_j}} - \frac{\partial \mathrm{U_j}}{\partial \mathrm{x_i}})^2} \tag{8}$$

In this work we compared for one case with the bars in tandem arrangement principally the predictions of local and global heat transfer coefficient on the channel walls with both k-ε models. The standard constants are employed: C_μ = 0.09, C_1 = 1.44, C_2 = 1.92, σ_k = 1.0, σ_ε = 1.3, Pr_t = 0.9 (Launder and Spalding, 1974).

Near-wall treatment

Wall functions given by Launder and Spalding (1974) are employed to prescribe the boundary conditions along the faces of the two bars and the channel walls of the computational domain. For the regions around the bars the law of the wall is assumed to be valid for the flow, and for the regions near the channel walls the law of the wall is assumed to be valid for both the flow and temperature fields. The wall functions are applied in terms of diffusive wall fluxes. For the wall-tangential moment these are the wall shear stresses and the non-dimensional wall distance y^+ defined as:

$$\tau_w = \frac{\rho U_p C_\mu^{1/4} k_p^{1/2} \kappa}{\ln(E y^+)} \qquad y^+ = \frac{\rho y_p C_\mu^{1/4} k_p^{1/2}}{\mu} \tag{9}$$

If $y^+ \leq 11.6$ the wall shear stress is calculated with the laminar equation. The subscript p refers to the grid point adjacent to one wall. The production rate of k and the averaged dissipation rates over the near-wall cell for the k-equation as well as the value of ε at the point p are computed respectively from the following equation:

$$P_K = \tau_w \frac{U_p}{y_p} \qquad \bar{\varepsilon} = \frac{C_\mu^{3/4} k_p^{3/2}}{\kappa y_p} \ln(E y^+) \qquad \varepsilon_p = \frac{C_\mu^{3/4} k_p^{3/2}}{\kappa y_p} \tag{10}$$

For the temperature boundary condition, the heat flux to one channel wall is derived from the thermal wall function:

$$q_w = \frac{(T_w - T_p)\rho C_P C_\mu^{1/4} k_p^{1/2}}{Pr_t(\ln(E y^+)/\kappa + P)} \tag{11}$$

where the empirical function P is specified as:

$$P = \frac{\pi/4}{\sin(\pi/4)} \left(\frac{A}{\kappa}\right)^{1/2} \left(\frac{Pr}{Pr_t} - 1\right) \left(\frac{Pr_t}{Pr}\right)^{1/4} \tag{12}$$

The channel walls are subjected to a constant wall temperature T_w in the present simulations. The bars do not have imposed temperature, and the heat transfer surfaces are the same as in the plane channel without mounted bars. Local Nusselt numbers on the channel walls were computed with the following equation:

$$\mathrm{Nu(x)} = \frac{\mathrm{h(x)H}}{\mathrm{k}} = \frac{\mathrm{q_w\ H}}{\mathrm{k(\ T_w - }\mathit{T}_\mathrm{b}\mathrm{(x))}} \tag{13}$$

The flow losses were evaluated with the apparent friction coefficient f defined as:

$$f = \frac{\Delta \mathrm{PH}}{1/2\rho \mathrm{U_0^2 2L}} = 1/2(\mathrm{C_{f1}} + \mathrm{C_{f2}}) + \mathrm{C_{D1}}\frac{\mathrm{d}}{2\mathrm{L}} + \mathrm{C_{D2}}\frac{\mathrm{d}}{2\mathrm{L}} - \Delta\beta\frac{\mathrm{H}}{\mathrm{L}} \tag{14}$$

where C_{f1} and C_{f2} are the skin friction coefficients on the channel walls, C_{D1} and C_{D2} are the drag coefficients of the bars mounted in the channel, and $\triangle\beta$ is the variation of the velocity factor. The skin friction coefficient, drag coefficient and velocity factor are defined as:

$$\mathrm{C_f} = \frac{\tau_\mathrm{w}}{1/2\rho \mathrm{U_o}^2} \qquad \mathrm{C_D} = \frac{\mathrm{D}}{1/2\rho \mathrm{U_0}^2 \mathrm{d}} \qquad \beta = \frac{1}{\rho \mathrm{U_0}^2 \mathrm{H}} \int_0^\mathrm{H} \rho \mathrm{u}^2 \mathrm{dy} \tag{15}$$

The apparent friction coefficient f is calculated by C_f, C_D, and β through equation (14) in each temporary iteration in the computational domain.

Additionally we calculate the lift coefficient and the Strouhal number defined by:

$$\mathrm{C_L} = \frac{\mathrm{L}}{1/2\rho \mathrm{U_0}^2 \mathrm{d}} \quad \mathrm{St} = \frac{\mathrm{fd}}{\mathrm{U_0}} \tag{16}$$

where L denotes lift and f denotes frequency of the flow.

Geometry and boundary conditions

The computational domain and the boundary conditions are sketched in Figure 1. Figure 1a shows the tandem arrangement of the square bars in the channel, and the Figure 1b shows the side by side arrangement of the bars to the approaching flow. At the inlet, the flow enters with only a streamwise component U_0 uniform, the Reynolds numbers, $Re=U_0H/\upsilon$, based on the channel height is 10^4, and a turbulence level of $Tu=ú/U_0=0.02$ is prescribed at the inlet. The bars size, d/H, has a fixed value of 0.152. Valencia (2000) has found that the Nusselt number increases in linear form with the bar size but the flow losses increase in exponential form, for this reason a small bar size is chosen. The channel length is only 5H, because we want to study the effects of the interaction of the two bars on flow losses and heat transfer on the channel walls. The longitudinal spacing between bars' centers G_L was varied between: 5.5d, 6.665d, 7.75d, 8.875d, and 10d. The transverse spacing between bars centers G_T was varied between: 2d, 2.53d, 3.58d, and 4d. The case with one mounted square bar was also simulated as reference: $G_L=G_T=0$.

A ratio of $\mu_t/\mu = 10$ is assumed to compute the inflow value of the dissipation rate ε. In general, the possible inlet flow conditions toward a

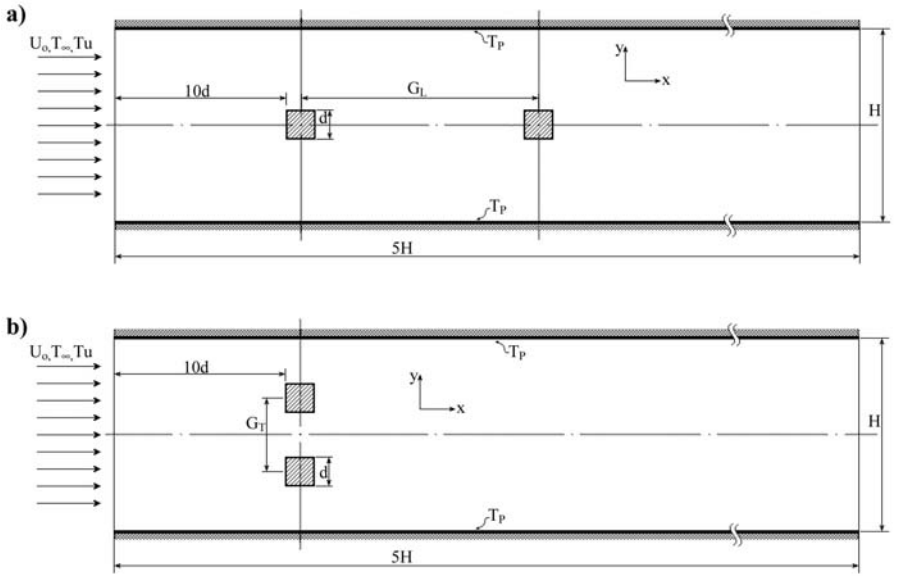

Figure 1.
Computational domain
(a) tandem arrangement;
(b) side by side

channel for U, V, k, ε and μ_t are several. In the present study, the inlet flow conditions are prescribed according to those described in the work of Bosch and Rodi (1996).

A detailed investigation of the appropriate exit condition was undertaken. It was found that the wave equation at the outlet and the streamwise gradients of all variables set to zero gave the same results. The distortion of the unsteady vortices shed from the downstream bar in the tandem arrangements was small.

Numerical solution technique

The differential equations introduced above were solved numerically with an iterative finite-volume method, details of which can be conveniently found in Patankar (1980). The convection terms in the equations were approximated using a power-law scheme. The method uses staggered grids and Cartesian velocity components, handles the pressure-velocity coupling with the SIMPLEC algorithm in the form given by Van Doormaal and Raithby (1984), and solves the resulting system of difference equations iteratively with a tridiagonal-matrix algorithm. A first-order accurate fully implicit method was used for time discretization in connection with a relatively small time step $\triangle\pi = \triangle tU_0/H = 0.0025$. A typical run of 12,000 time steps with 625 $\times$ 125 grid points takes about 1×10^4 CPU minutes on an IBM RISC 6000 397 workstation (peak performance 0.5 GFLOPS). To determine means values the program should be run until a periodic state is reached, and then the values of all fields in each 1/16 of one period are saved.

Results and discussion

To check grid independence in this work the case with one mounted square bar in the channel, $Re = 10^4$, $d/H = 0.152$, $L/H = 5$, $G_T = G_L = 0$, was simulated with the standard k-ε turbulence model for five grid sizes. Values of integral parameters as the mean drag coefficient, mean skin friction coefficient, mean Nusselt number on the channel wall, apparent friction coefficient, and eddy-shedding Strouhal number of the flow are compared in Table I. The mean Nusselt number and apparent friction coefficient calculated with the standard k-ε turbulence model for the turbulent developing channel flow without a mounted square bar is also shown in Table I for the five different grids.

From Table I one can observe that with the grids of 625 × 125 control volumes the damping effect of the grid size is very small compared with the grids of 750 × 150 control volumes. Therefore the grids with 625 × 125 control volumes will be used in this work for the correct simulation of the unsteady turbulent flows around the bar arrangements in the channel, with this grid size are the variations of the calculated integral parameters smaller than 3 per cent compared with the finest grid size. The dimensionless, sublayer-scaled wall distance of the first grid point, y_p^+, varies with the distance along the channel and with the used mesh size, in this work the laminar case $y_p^+ < 11.6$, and the turbulent case $y_p^+ > 11.6$, has been programmed in the wall function formulation. Thus, the results with the different used grid sizes do not show an influence of this factor. Another important aspect is that the calculation time with the finest grid size is increased two-fold compared with the grid of 625 × 125 control volumes.

Finally, the same case with one mounted square bar in the channel $Re = 10^4$, $d/H = 0.152$, $L/H = 5$, $G_T = G_L = 0$, was simulated with the grid of 625 × 125 control volumes and with a finer time step of $\triangle\tau = 0.00125$, the variations of all the averaged parameters were smaller than 2 per cent, therefore the time step of $\triangle\tau = 0.0025$ will be used in all the calculations.

The modified version of the standard k-ε turbulence model proposed by Launder and Kato (1993) intensifies the Karman vortex sheets behind the bar by means of a reduction of the turbulent kinetic energy k around the bar. However, a comparison between the local heat transfer coefficient on the channel wall calculated with the standard k-ε turbulence model and the LK model for the tandem arrangement with $G_L/d=10$ shows small differences, due to the fine grid used in this work. For this reason in this work we use for the rest of the simulations the standard k-ε turbulence model.

Grid	C_D	$C_f \times 1{,}000$	Nu	$f \times 1{,}000$	St	Nu_0	$f_0 \times 1{,}000$
300 × 60	1.787	14.47	54.00	47.34	0.168	51.02	18.00
400 × 80	1.803	15.38	55.97	47.85	0.173	52.86	19.31
500 × 100	1.832	16.18	57.58	49.65	0.172	54.14	20.34
625 × 125	1.846	16.88	58.82	51.36	0.167	54.92	21.06
750 × 150	1.852	17.34	59.40	52.26	0.164	55.26	21.44

Table I. Average values for different grid sizes, $Re = 10^4$, $d/H = 0152$, model k-ε standard

The structure of the unsteady turbulent flow in the channel with two square bars mounted on the channel axis in tandem arrangement, and with the two bars arranged side by side to the flow, calculated with the standard k-ε model will be discussed. It will be illustrated through the use of computed instantaneous velocity vectors and contours of the turbulent kinetic energy with the grid of 625×125 control volumes and a time step $\triangle\tau = 0.0025$.

Figure 2 shows instantaneous maps of fluctuating velocity vectors and contours of the turbulent kinetic energy for two tandem arrangements G_L = 5.5d and G_L = 8.875d for the same phase t/T = 0.25 in the channel. Figure 2 shows that vortex sheets are alternately shed by the upstream bar and these travel diagonally through the gap, washing across the upstream face of the downstream bar. Thus, the upstream surface of the downstream bar is exposed to a periodic flushing condition induced by the upstream bar. The downstream bar amplifies the intensity of the detachment of vortices. The contours of the turbulent kinetic energy or Reynolds normal stresses are associated with local maxima of vorticity, thus the k-contours in Figure 2 show the intensity of the unsteady vortices. The values of k are bigger around the downstream bar.

In the tandem arrangements the mean drag coefficient of the downstream bar increases with the longitudinal separation distance, and the mean drag coefficient reaches similar values of the upstream bar for G_L = 10d (Table II). The mean skin friction coefficient on the channel walls and the Strouhal number change slightly with GL. The frequency of eddy shedding is the same as in the arrangement with one mounted square bar (Table I).

Figure 3 shows instantaneous maps of fluctuating velocity vectors and contours of the turbulent kinetic energy for two arrangements of bars arranged side by side to the flow G_T = 2.53d and G_T = 3.58d for the same phase t/T=0.25 in the channel. Figure 3 shows that vortex sheets are alternately shed by the bars in-phase form with G_T = 2.53d and in an anti-phase form with G_T = 3.58d. However, in Figure 3a one can observe that the unsteady flows behind the bars are not the same, the intensity of the Karman vortex sheets behind the superior bar is smaller than in the inferior bar. We call superior and inferior bar, superior and inferior channel wall in reference to the position of the bars and the channel walls with the entrance of the turbulent flow in the computational domain shown in Figure 1b.

The flow mode changes with the bar separation distance G_T and therefore with the distance of the bar from the channel wall, the flow is anti-phase with G_T = 2d and in-phase with G_T = 4d (Table III). In this configuration a complex interaction exists among the presence of the channel wall and the transverse separation distance between the bars in the generation of the unsteady vortices behind the bars.

The mean drag coefficients of both bars are similar and much bigger than in the tandem arrangements, with the bars arranged side by side the mean lift coefficients of the bars are not zero. In the arrangements with G_T/d = 2 and 2.53 the bars have a force of repulsion, with bigger G_T/d the bars have a force of attraction. The Strouhal number changes also with the separation distance of

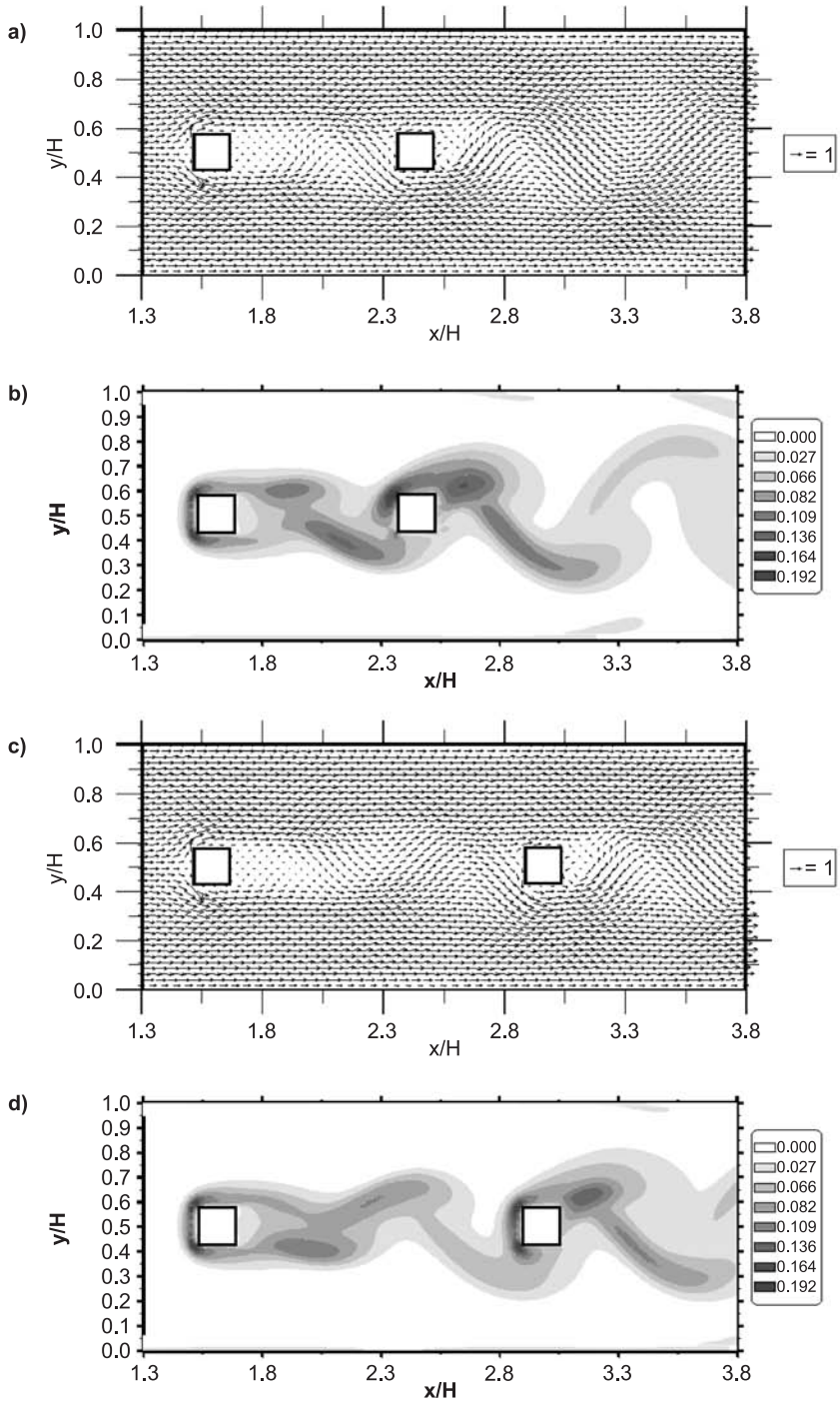

Figure 2.
Instantaneous maps of velocity vectors and contours of turbulent kinetic energy for tandem arrangements (a) and (b) $G_L/d=5.5$; (c) and (d) $G_L/d=8.875$

the bars and the frequency of eddy shedding in this case is bigger than with the bars arranged in tandem (Table III). The blockage ratio of the channel is not the same in both situations, and this parameter is very important in the behavior of the fluid in the channel. The mean values of the skin friction coefficients are also different in the superior and inferior channel walls.

Figure 4 shows the influence of the unsteady vortices on computed instantaneous local Nusselt number at the inferior channel wall for a tandem arrangement with $G_L/d = 8.875$ (Figure 4a) and with the bars arranged side by side to the approaching flow with $G_T/d = 3.58$ (Figure 4b). The strong local variations are due to the unsteady washing of the wall by the transverse vortices shown in Figures 2 and 3. In the tandem arrangement the local heat transfer increases strongly after 1H, the big temporal variations of the Nusselt number after 2H are due to the alternately shed of vortex sheets. In the arrangement with the bars placed side by side to the flow (Figure 4b), the local heat transfer increases strongly due to the blockage of the channel at 1.52H, the local Nusselt number decreases in this case after 3H. In this case the flow is in anti-phase form. The amplitude of the temporal variations of the Nusselt number in one period is smaller than in the tandem arrangement of the bars after 3H. In both arrangements the influence of the periodically shedding vortices from the bars reaches the whole channel behind the bars.

The time averaged local skin friction coefficient distributions on the channel walls are shown in Figure 5 for the five studied tandem arrangements (Figure 5a), and for the four side by side arrangements of the square bars calculated with the standard k-ε turbulence model. The local skin friction coefficient takes a maximum both at the inserted position of the first bar and at the position of the downstream bar in the tandem arrangements. In the arrangements with the bars mounted side by side to the flow, the maximum of the skin friction coefficient is much bigger that in the tandem arrangements, and decreases fast after the bars' location in the channel. In both figures the local distribution of the skin friction coefficient for the case with only one mounted square bar in the channel, $G_L = G_T = 0$, and for the plane channel are shown for comparison.

Figure 6 compares the time averaged Nusselt number distributions for the five cases with the bars arranged in tandem (Figure 6a), and for the four cases with the bars arranged side by side (Figure 6b). In the tandem arrangements (Figure 6a), the local Nusselt number takes a local maximum at the inserted position of the upstream bar, and at the inserted position of the downstream

Table II.
Mean values of drag coefficient, skin friction coefficient and Stouhal number for different longitudinal spacing G_L

G_L/d	C_D bar upstream	C^D bar downstream	$C_f \times 1{,}000$	St
5.5	1.84	1.25	18.08	0.163
6.665	1.85	1.48	18.26	0.164
7.75	1.85	1.59	18.38	0.166
8.875	1.84	1.64	18.48	0.166
10.0	1.85	1.70	18.55	0.167

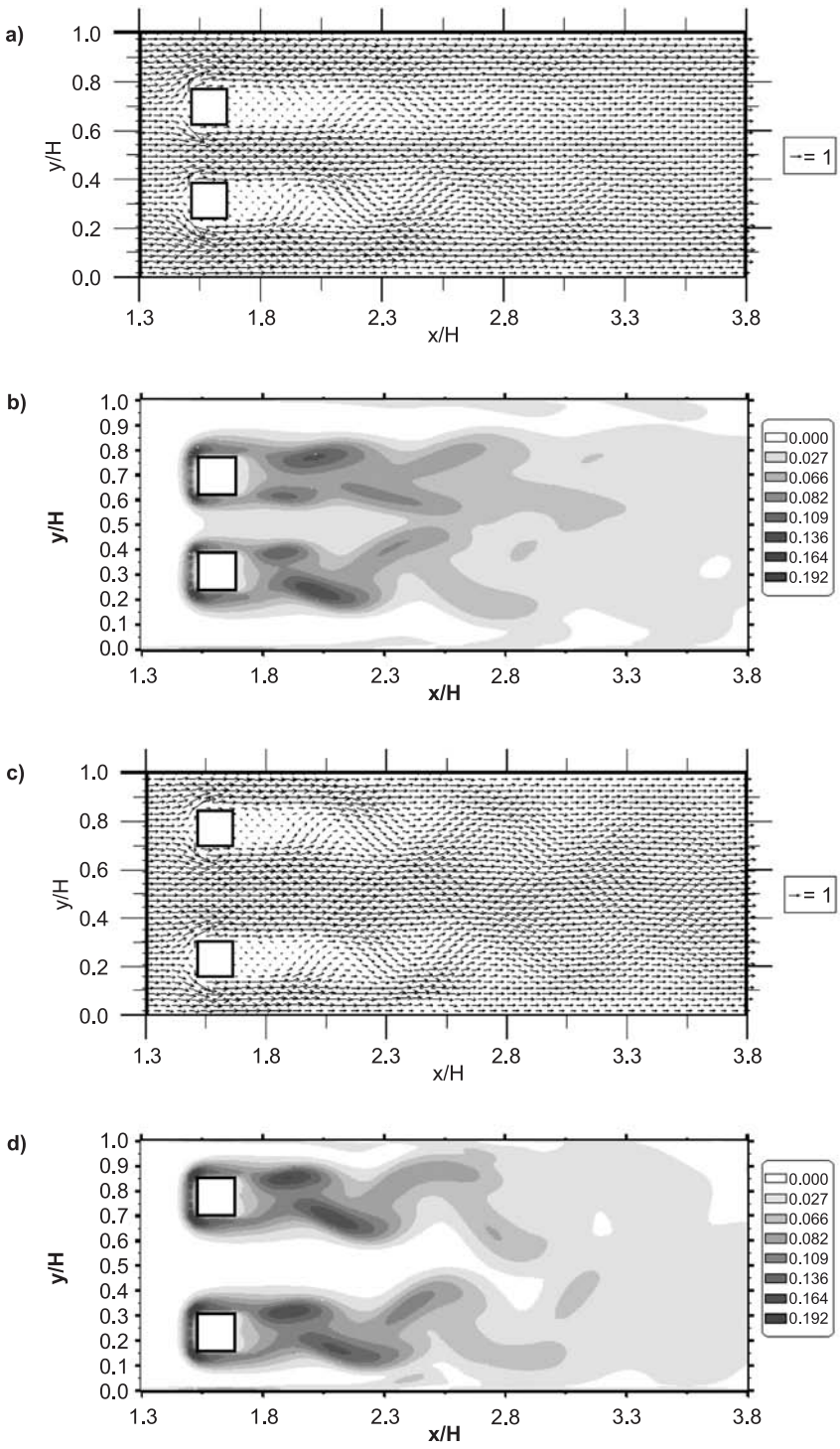

Figure 3.
Instantaneous maps of velocity vectors and contours of turbulent kinetic energy for bars arranged side by side to the flow (a) and (b) $G_T/d=2.53$; (c) and (d) $G_T/d=3.58$

bar, after the second bar the Nusselt number increases strongly due the effect of the periodically shedding vortices from the bars. With the bars arranged side by side (Figure 6b), the first local maximum of the Nusselt number results from flow acceleration due to the blockage effect of the two bars, while the second local maximum is caused by the periodically shedding vortices from the bars. In these arrangements the local Nusselt number decreases at the exit with G_T. The Nusselt number distribution for the case with only one mounted square bar in the channel, $G_L=G_T=0$, and for the plane channel are also shown for comparison.

Figure 7 compares the mean Nusselt number on the channel walls and apparent friction coefficient against the longitudinal separation distance GL (Figure 7a), and against the transverse separation distance GT (Figure 7b). With the bars arranged in tandem the mean Nusselt number has a maximum for $G_L/d = 7.75$, however the apparent friction coefficient increases almost lineally with G_L. With the bars arranged side by side to the flow, the form of the dependence of the Nusselt number and the apparent friction coefficient with G_T is not so marked. The most favorable case is for $G_T/d = 3.58$, so the enhancement of mean heat transfer is 29 percent, this heat transfer enhancement is associated with an increase on the apparent friction coefficient ratio of 5.2.

Conclusions

The unsteady turbulent flow of air and heat transfer in a channel with two mounted square bars in different arrangements were numerically simulated with the standard k-ε turbulence model. Five arrangements with the bars mounted in tandem along the channel axis and four cases with the bars arranged side by side to the approaching flow were studied. In the tandem arrangements, the downstream bar intensifies the detachment of vortices and therefore the mean local heat transfer increases strongly after the second bar. With the bars arranged side by side to the flow, anti-phase and in-phase unsteady flow behavior were found as function of the transverse separation distance of the bars. The mean enhancement of heat transfer was considerably smaller than the increase of the pressure drop in both types of arrangements.

Table III.
Mean values of drag, lift, skin friction coefficient and Stouhal number for different transverse spacing G_T. A: anti-phase I: in-phase

G_T/d	C_D bar superior	C_D bar inferior	C_L bar superior	C_L bar inferior	$C_f \times 1{,}000$ superior	$C_f \times 1{,}000$ inferior	St	Flow mode
2.0	2.87	2.87	0.43	–0.43	22.19	22.19	0.220	A
2.53	2.70	2.81	0.18	–0.26	21.76	21.48	0.251	I
3.58	2.71	2.70	–0.07	0.08	19.72	19.80	0.234	A
4.0	2.72	2.72	–0.19	0.19	19.23	19.26	0.239	I

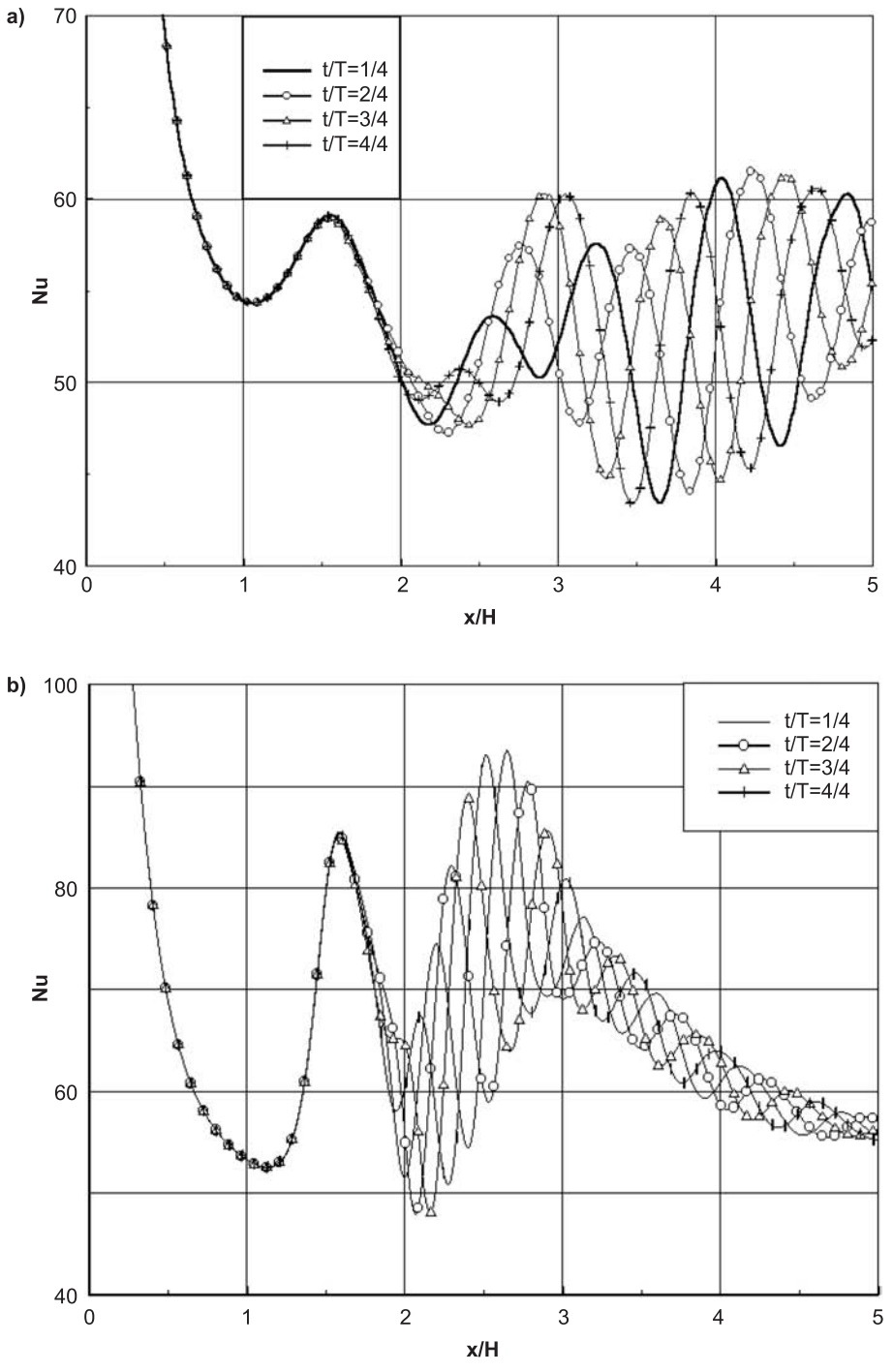

Figure 4.
Instantaneous local Nusselt number on the channel wall for four phases, (a) tandem arrangement $G_L/d=8.874$ (b) bars arranged side by side $G_T/d=3.58$

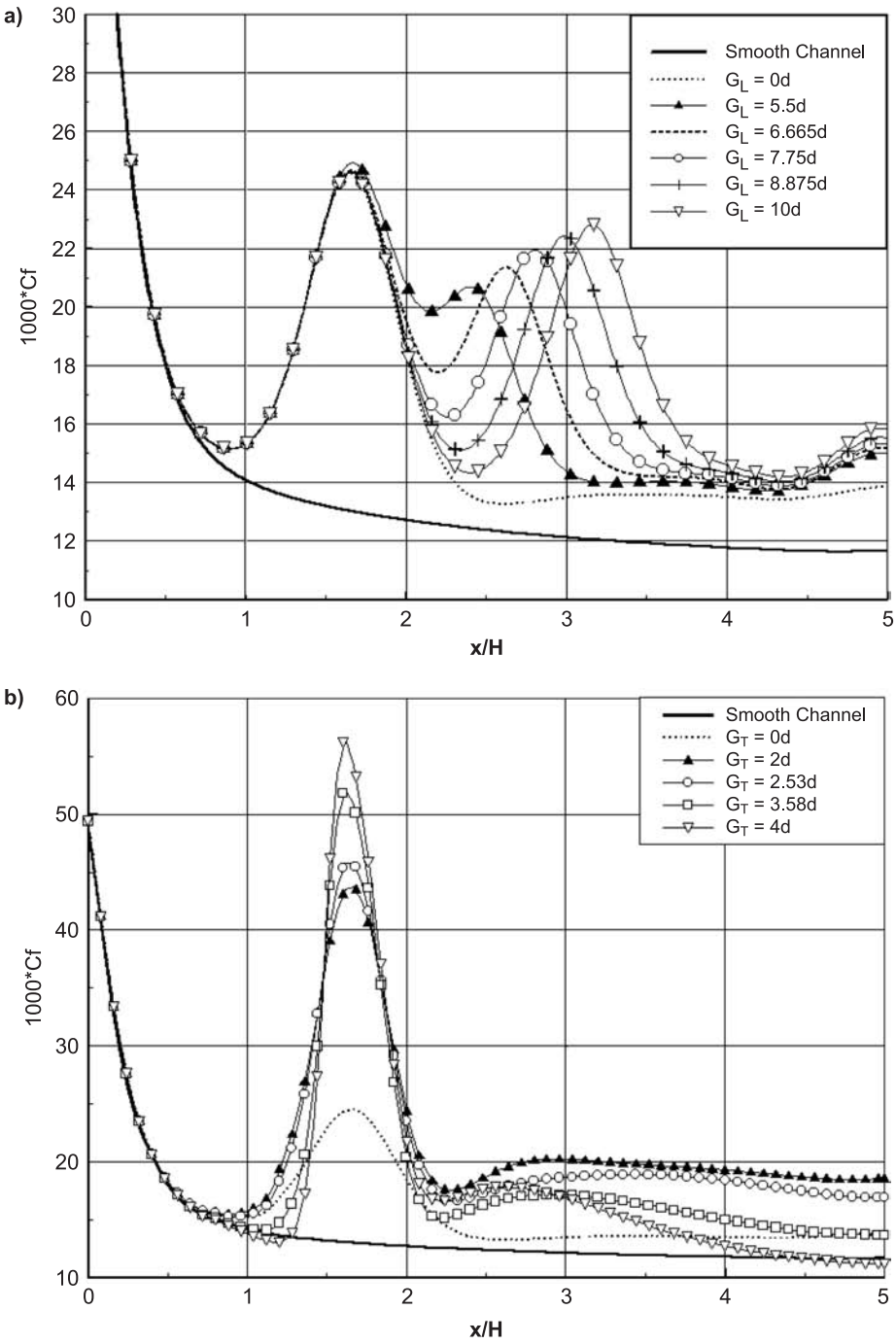

Figure 5.
Time-averaged local skin friction coefficient (a) tandem arrangements, (b) side by side arrangments

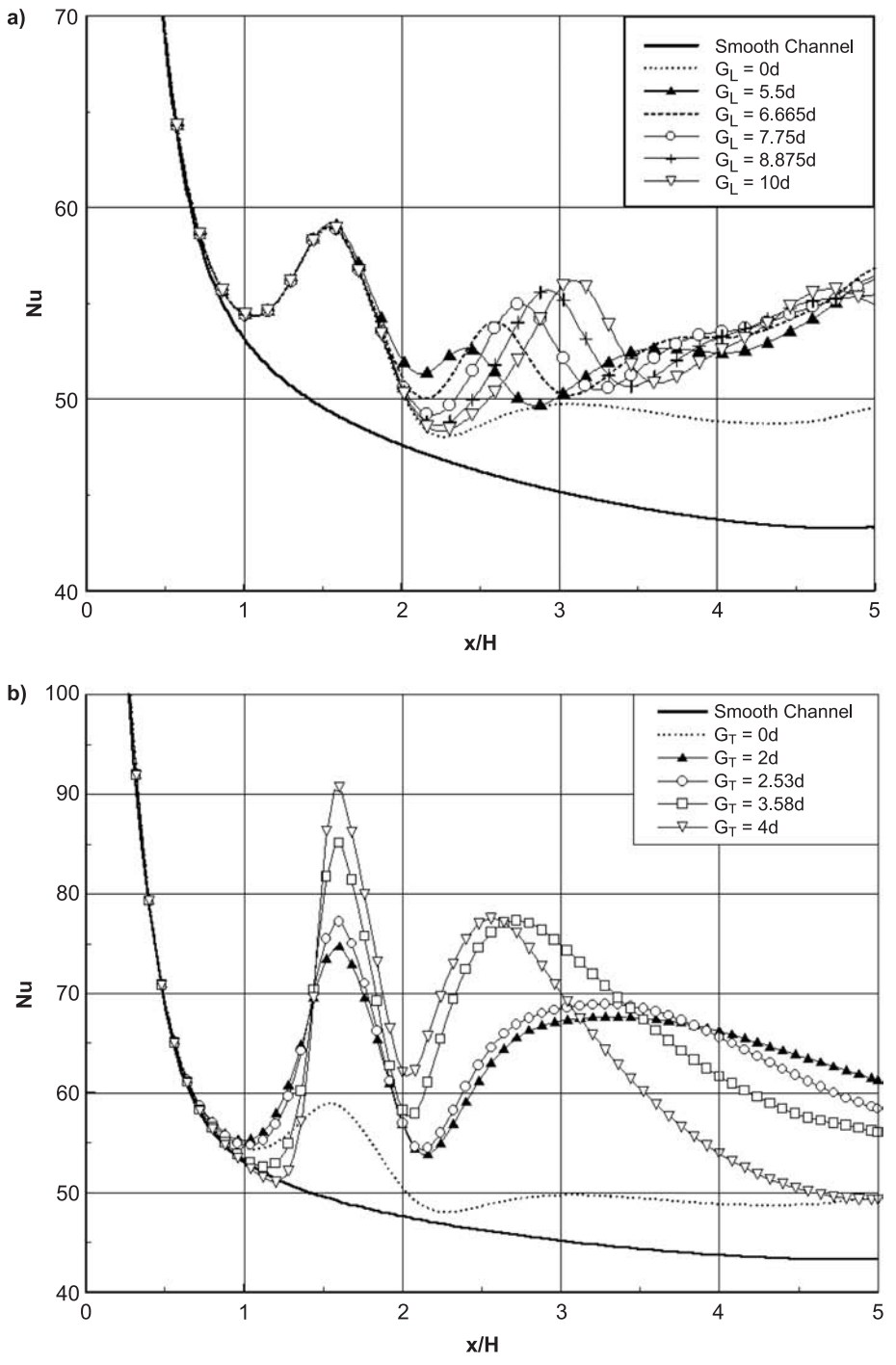

Figure 6.
Time-averaged local Nusselt number (a) tandem arrangements (b) side by side arrangements

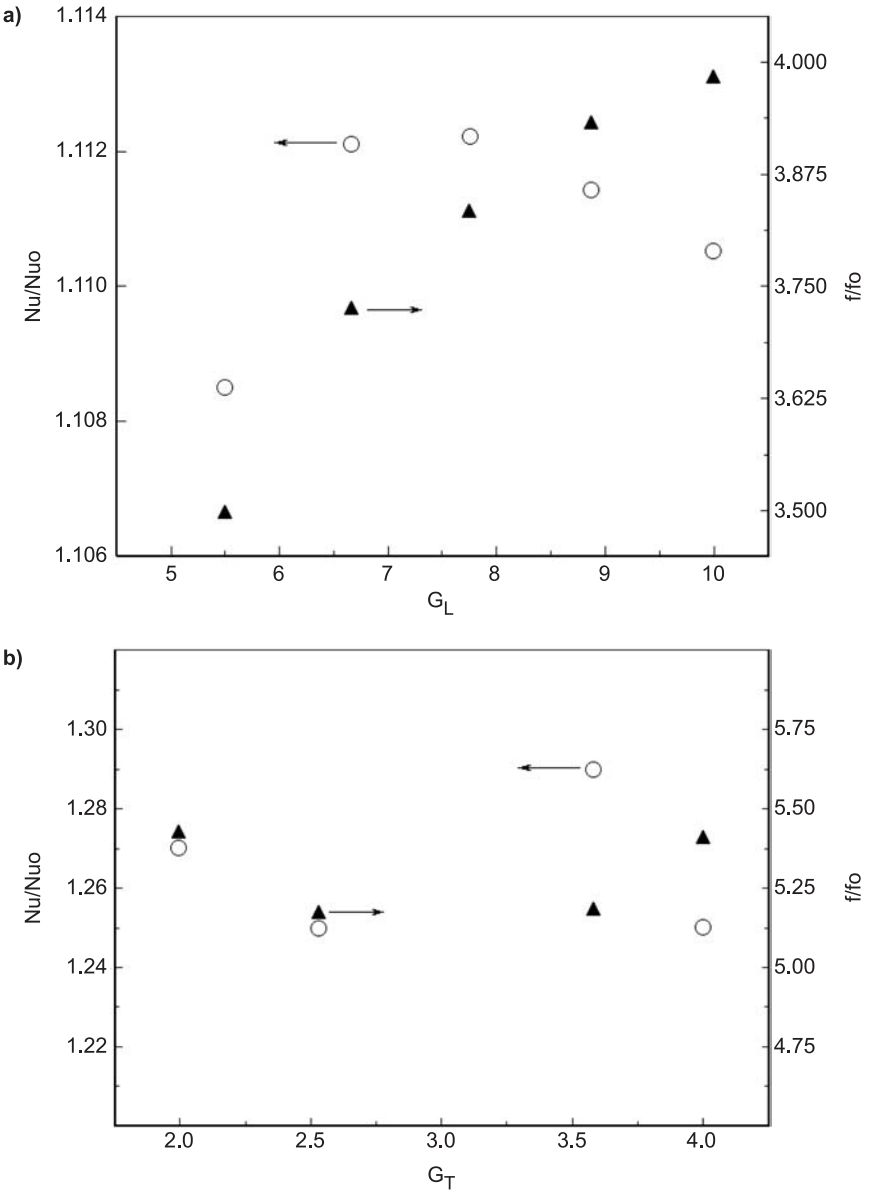

Figure 7.
(a) Nusselt number and apparent friction coefficient against G_L/d
(b) Nusselt number and apparent friction coefficient against G_T/d

References

Bosch, G. and Rodi, W. (1996), "Simulation of vortex shedding past a square cylinder near a wall", *International Journal of Heat and Fluid Flow*, Vol. 17, pp. 267-75.

Bosch, G., Kappler, M. and Rodi, W. (1996), "Experiments on the flow past a square cylinder placed near a wall", *Experimental Thermal and Fluid Science*, Vol. 13, pp. 292-305.

Cho, H.H., Jabbari, M.Y. and Goldstein, R.J. (1994), "Mass transfer with flow through an array of rectangular cylinders", *ASME Journal of Heat Transfer*, Vol. 116, pp. 904-11.

Durão, D.F.G., Gouveia, P.S.T. and Pereira, J.C.F. (1991), "Velocity characteristics of the flow around a square cross section cylinder placed near a channel wall", *Experiments in Fluids*, Vol. 11, pp. 341-50.

Ishigai, S., Nishikawa, E., Nishimura, K. and Cho, K. (1972), "Experimental study of gas flow in tube banks with tube axes normal to flow", *Bulletin of the JSME*, Vol. 15, pp. 949-56.

Launder, B.E. and Kato, M. (1993), "Modelling flow-induced oscillations in turbulent flow around a square cylinder", *Unsteady Flow*, FED-Vol. 157, ASME, pp. 189-99.

Launder, B.E. and Spalding, D.B. (1974), "The numerical computation of turbulent flows", *Computer Methods in Applied Mechanics and Engineering*, Vol. 3, pp. 269-89.

Liou, T.M. and Chen, S.H. (1998), "Turbulent flow past an array of bluff bodies aligned along the channel axis", *ASME Journal of Fluids Engineering*, Vol. 120, pp. 520-30.

Nakagawa, S., Senda, M., Hiraide, A. and Kikkawa, S. (1999), "Heat transfer characteristics in a channel flow with a rectangular cylinder", *JSME International Journal Series B*, Vol. 42, pp. 188-96.

Patankar, S.V. (1980), *Numerical Heat Transfer and Fluid Flow*, Hemisphere, New York, NY.

Tatsutani, K., Devarakonda, R. and Humphrey, J.A.C. (1993), "Unsteady flow and heat transfer for cylinder pairs in a channel", *International Journal of Heat and Mass Transfer*, Vol. 36, pp. 3311-28.

Valencia, A. (2000), "Turbulent flow and heat transfer in a channel with a square bar detached from the wall", *Numerical Heat Transfer Part A*, Vol. 37, pp. 289-306.

Van Doormaal, J.P. and Raithby, G.D. (1984), "Enhancements of the SIMPLE method for predicting incompressible fluid flows", *Numerical Heat Transfer*, Vol. 7, pp. 147-63.

Zdravkovich, M.M. (1977), "REVIEW – Review of flow interference between two circular cylinders in various arrangements", *ASME Journal of Fluids Engineering*, Vol. 99, pp. 618-33.